The 2000 Institute of Metals Lecture
The Minerals, Metals & Materials Society

Some Generalities in the Analyses of Equilibria in Ionic Solutions

ROBERT A. RAPP

ROBERT F. MEHL
AWARD MEDALIST

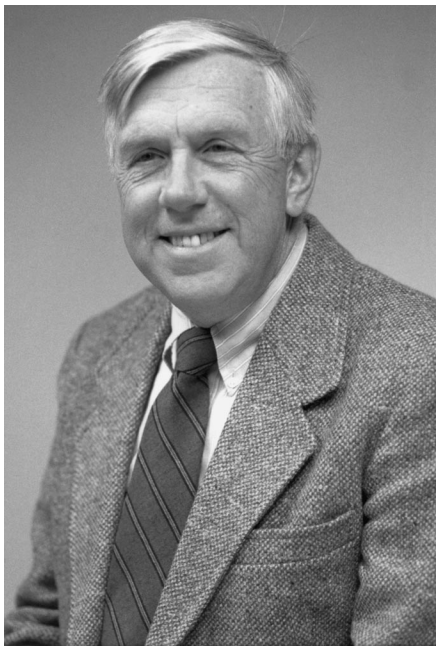

Despite great differences in the physical and chemical properties of various ionic media, common methods for analyzing internal equilibrium provide useful and simple means for interpreting and predicting their behavior. The formalism of M. Pourbaix for analyzing the activities and solubilities of solutes in aqueous solutions has provided a foundation for interpreting corrosion, solubilities, and electrochemical phenomena for such solutions. Although perhaps not so obvious, the formalism of Kroger–Vink (K–V) in plotting the point defect concentrations for ionic solids derives from the same mathematical method. Likewise, the activities and solubilities for solutes in fused salts, *e.g.*, fused sodium sulfate, can be treated by exactly the same sort of simultaneous resolution of equilibria for reactions in an ionic medium. Suggestions for extension of this analysis to cryolite-base fused salt solutions important to aluminum extraction are discussed.

I. INTRODUCTION

PRIOR to addressing the technical aspects of this Institute of Metals Lecture, may I mention a few personal matters relative to my selection to receive the R.F. Mehl Medal. I was a graduate student in the Department of Metallurgical Engineering at Carnegie Institute of Technology during Professor Mehl's last years as Professor and Chairman. I was a student in the courses on Diffusion and Phase Transformations that he taught, and I remember well the knowledge, teaching methodology, and scientific principles that he

The Institute of Metals Lecture and Robert Franklin Mehl Award is presented for leadership in the field of materials science and applications. This honor recognizes an outstanding scientific leader by inviting him or her to present a lecture, at the Society's Annual Meeting, on a technical subject of particular interest to members in the materials science and application of metals program areas.

Dr. Robert A. Rapp, Distinguished University Professor Emeritus at Ohio State University's Department of Materials Science and Engineering, is The Minerals, Metals and Materials Society's (TMS) 2000 Institute of Metals Lecturer and will receive the Robert Franklin Mehl Award at the 2000 TMS Annual Meeting.

Dr. Rapp earned his B.S. from Purdue University in 1956 and his M.S. and Ph.D. from the Carnegie Institute of Technology in 1958 and 1959, all in metallurgical engineering. Dr. Rapp was a research metallurgist at Wright Patterson Air Force Base before joining the faculty at Ohio State.

He has published over 245 papers and holds 20 patents. Dr. Rapp was a Guggenheim Fellow from 1972 to 1973, has held two Fulbright scholarships, and is a fellow of six US and foreign societies. He is a member of the National Academy of Engineering.

Presentation of this award took place at the 2000 TMS Annual Meeting and Exhibition in Nashville, TN March 12–16. 2000.

imparted. He represented a professional role model that many graduates have admired and emulated. I am very proud and grateful for the opportunity to present this lecture dedicated to the memory of Professor Mehl.

For this Lecture, I have chosen to address and inter-relate some matters of thermodynamic analyses that are generally considered separate subjects, so that if the text should seem wide-ranging and disjointed, at least along the way but hopefully not at the end, then I have accomplished my goal. Indeed, I hope to show that several different sorts of analogies can be applied in treating the thermodynamics of widely different types of ionic solutions, especially to achieve useful graphical representations. This approach could be considered as a "framework" for understanding and advancing the knowledge about the subject, and I would suggest that this framework might serve as a good teaching tool. The several subjects will be presented in a sort of chronological sequence, according to their appearance in the literature.

(1) Pourbaix approach to aqueous solutions
   (a) Phase stability for the solvent and its solutes
   (b) Solubilities of oxides as a function of solution parameters
(2) Kroger–Vink (K–V) description of defects in solid compounds
   (a) Pure and doped ionic conductors
   (b) Pure and doped electronic conducting semiconductors
(3) Thermodynamic description of fused salt chemistry
   (a) Sodium sulfate-base solutions (one cation, multiple anions)
   (b) Defining, quantifying, and measuring the acid-base character for solutions
   (c) Solubilities of oxides as a function of solution parameters, effect of strong acid solute
   (d) Alkali sulfate-base solutions (one anion, multiple cations)
(4) Extension of the formalism to cryolite-base fluoride solutions
   (a) Phase stability for the Na-Al-F system
   (b) Definition and measurement of acid-base character
   (c) Oxide solubilities in cryolite solutions

Because of the limitations in space and time, I have intentionally chosen to present only quite simple illustrations, but I shall mention some complexities that may also be treated. Likewise, to restrict the length, I cannot point out most of the interesting and important engineering applications and technical implications for the several topics discussed. However, a few examples of practical applications of the analyses to the subject of Hot Corrosion are mentioned.

II. POURBAIX APPROACH TO EQUILIBRIUM IN AQUEOUS SYSTEMS

In his "doctorate thesis" from the Technical University of Delft in 1945, Marcel Pourbaix introduced a novel procedure for understanding equililibria in aqueous solutions by graphical representations involving the two principal solution parameters: oxidation potential ($RT \log P_{O_2}$) and acidity ($-\log a_{H^+}$). Since the former is measured by an electrochemical reference electrode, the oxidation potential is plotted on a linear scale as the "electrode potential" E. Likewise, the solution acidity, also measurable by an electrochemical reference electrode, is plotted on a linear scale as pH, but we should not forget that the "Pourbaix" diagram is essentially a log-log plot of phase stability. Within the Pourbaix formalism and framework, Figure 1 presents a simplified diagram describing phase stability for pure water,[1] the solvent for further considerations. At 25 °C, pure liquid water is stable over a wide regime of solution variables, but below line "a," water decomposes at equilibrium to liberate hydrogen (construction lines provide the alternative pressure values), and above line "b," the pressure of oxygen gas exceeds 1 atm so pure water at equilibrium is considered to decompose. The lines "a" and "b" are both sloping because they involve both an electron exchange and a reaction involving protons:

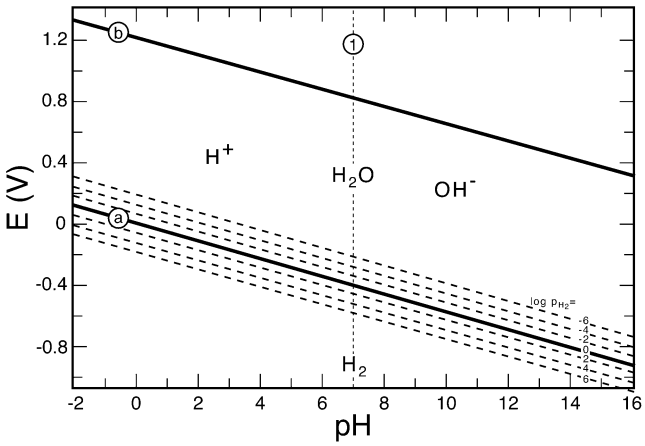

Fig. 1—Potential-pH equilibrium diagram for pure water at 25 °C.[1]

Line "a": $2H^+ + 2e^- = H_2\ (g)\ E^\circ = 0.000 - 0.0591pH - 0.0295 \log P_{H_2}$

Line "b": $2H_2O = O_2\ (g) + 4H^+ + 4e^-\ E^\circ = 1.228 - 0.0591pH + 0.0147 \log P_{O_2}$

The dashed vertical line "1" reflects the dissociation constant for water and separates the fields where either protons (on the left) or hydroxide ions (on the right) are the dominant ionic species. So, according to the Pourbaix approach, consideration of the pure solvent is the starting point for the examination of aqueous solutions containing solute ions. As an important experimental point, the simultaneous readings from two different reference electrodes are adequate to identify the exact local conditions at any working electrode in the aqueous solution.

As one possible example for application of this method to analyze the thermodynamic stability of a material in water, Figure 2 presents the Pourbaix diagram for the system copper-water at 25 °C, where Cu, Cu_2O, and CuO, but not $Cu(OH)_2$, are considered to be the stable solid phases. Then Figure 2 is a superposition of an "Ellingham" phase stability plot for the Cu-O-H system onto the water stability plot, thus treating the mutual stability of the two substances. The oxides Cu_2O and CuO can dissolve as either an acidic solute (Cu^{2+}) on the left of the diagram, or else as basic solutes ($HCuO_2^-$ or CuO_2^{2-}) on the right, while metallic copper dissolves essentially only as an acidic solute Cu^{2+}. The reactions describing the dissolution of CuO at relatively high electrode potentials are as follows.

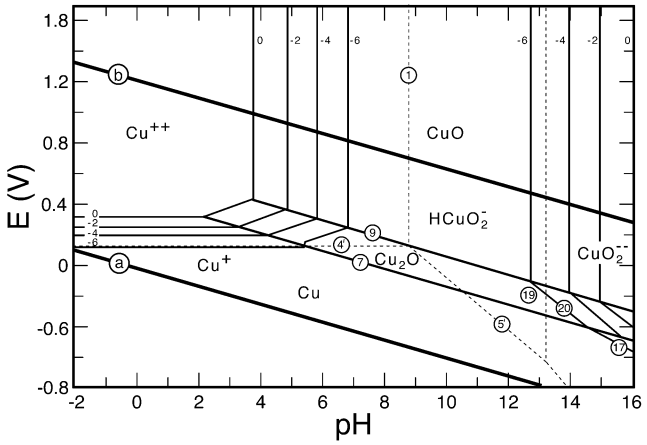

Fig. 2—Potential-pH equilibrium diagram for the copper-water system at 25 °C.[1]

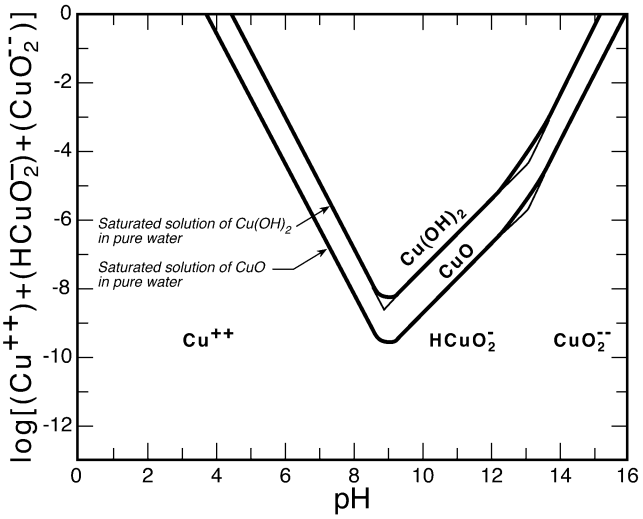

Fig. 3—Influence of pH on the solubilities of CuO and $Cu(OH)_2$ at 25 °C.[1]

At relatively high electrode potential:

$$\text{Basic dissolution: } CuO + H_2O = HCuO_2^- + H^+ \quad [1]$$

$$d \log [HCuO_2^-]/d\,(\text{pH}) = 1 \quad [1']$$

$$\text{In a very basic melt: } CuO + H_2O = CuO_2^{2-} + 2H^+ \quad [2]$$

$$d \log [CuO_2^-]/d\,(\text{pH}) = 2 \quad [2']$$

$$\text{Acidic dissolution: } CuO + 2H^+ = Cu^{2+} + H_2O \quad [3]$$

$$d \log [Cu^{2+}]/d\,(\text{pH}) = -2 \quad [3']$$

Similar expressions are readily worked out to treat the dissolution of Cu_2O at lower electrode potential.

In Figure 2, the limits of phase stability for the copper-containing phases are described by the lines marked 0, −2, −4, and −6 to denote solute activities of 1, 10^{-2}, 10^{-4}, and 10^{-6}, consistent with Eqs. [1′] through [3′]. For ideal solutions of the solute in the solvent, these values also correspond to the solute mole fractions. If activity coefficients are known for the solutes, the correlation of activity and concentration can be made. If the less stable compound $Cu(OH)_2$ had been plotted in Figure 2 instead of CuO, then the width of the $Cu(OH)_2$ field would be less than that for CuO.

Years ago, the construction of diagrams such as Figure 2 was done by hand at your desk, requiring only thermodynamic tables for the Standard Gibbs Energies of Formation for the phases involved; today Pourbaix diagrams are readily provided by computer software with a stored bank of thermodynamic data. Diagrams analogous to Figure 2 are available for nearly every metal of the periodic chart. Pourbaix's "Atlas of Electrochemical Equilibria in Aqueous Solutions,"[1] published in 1966 and revised in 1974, already provides a good coverage of these diagrams plus their application to corrosion problems in aqueous solutions.

The next logical consequence of such an analysis is illustrated by Figure 3, where the logarithm of the solubilities for both CuO and the less stable $Cu(OH)_2$ are plotted as a function of pH, assuming ideal solutions for the solutes. These calculated curves follow logically from Figure 2, and comprise an acidic "leg" for the Cu^{2+} solute with negative slope and two basic legs with differing positive slopes for the two basic solutes $HCuO_2^-$ and CuO_2^{2-}. The slopes of these "ideal" solubility curves are described by Eqs. [1′] through [3′]. The experimental realization of an oxide-water equilibrium is quite difficult at such low temperatures as 300 K. Therefore, solubility curves for most metal-oxygen systems in water have been calculated with the assumption of an ideal solution. Comparison of the solubility plots for CuO and $Cu(OH)_2$ in Figure 3 supports the known thermodynamic expectation that any less stable phase is more soluble in a solvent than a more stable phase.

This simplest outline of the Pourbaix formalism presented here has been extended to treat more complicated solutions such as strong acids, which complex with oxide ions; cation-complexing ions (*e.g.*, chloride or ammonium ions), which tie up metal solutes, *etc.*; and the temperature for the analysis has been raised greatly to treat pressurized water, *e.g.*, at 600 K. Such examples are illustrated in Reference 2, but they cannot be treated here.

III. K–V DESCRIPTION OF DEFECTS IN SOLID COMPOUNDS

Following the suggested existence of interstitial and vacancy defects in crystalline compounds by Frenkel[3] and Wagner and Schottky,[4] such point defects began to appear in equations describing chemical equilibria and their associated equilibrium constants. Although Wagner[5] had analyzed the dominant point defects for a broad range of compounds, *e.g.*, halides and oxides, with a full appreciation of the importance of the required balances for mass, lattice sites, and electrical neutrality, he had not offered graphical representations to describe all the possible point defect situations for a given compound. But a chapter by Kroger and Vink[6] and a book by Kroger[7] provided a format for treating internal equilibrium in crystalline compounds, as well as an improved notation system for describing point and electronic defects in crystalline compounds. The examples chosen for their analyses comprised sulfide, phosphide, and oxide compounds, which were of interest for optical properties and applications.

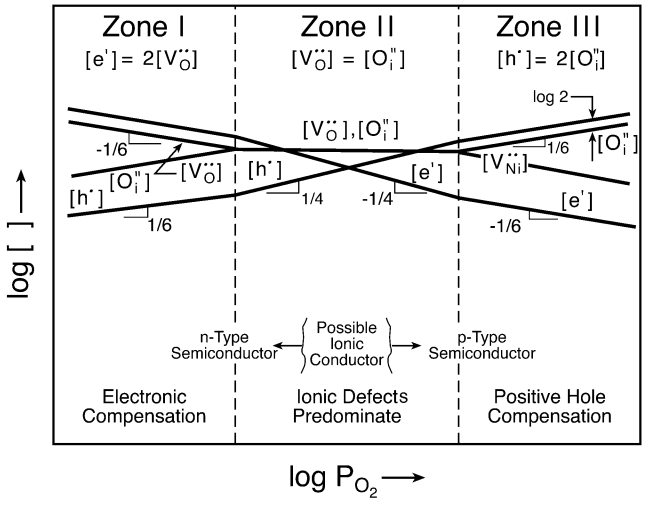

Fig. 4—K–V type diagram for defect concentrations in pure ThO_2.[9]

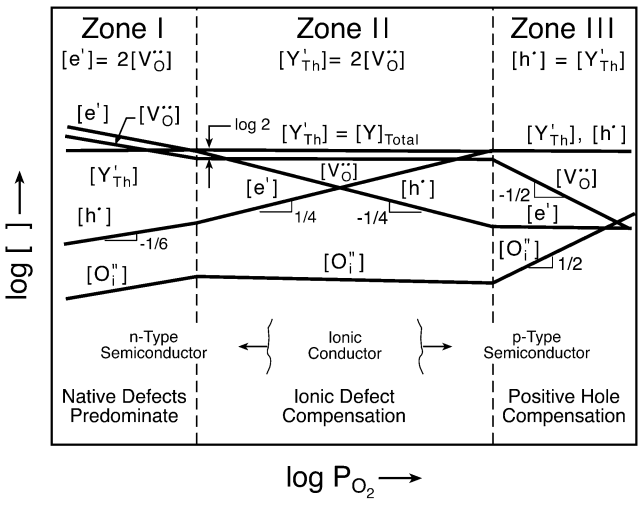

Fig. 5—K–V type diagram for defect concentrations in ThO_2-Y_2O_3 solid solutions.[9]

In the 1960s, K–V defect notation and equilibrium diagrams were introduced for oxides to analyze mixed ionic and electronic conduction in solid electrolytes, *e.g.*, for ThO_2 and ThO_2-Y_2O_3 solid crystalline solutions at high temperatures.[8,9] Figure 4 presents a Kroger–Vink log-log diagram for point defect concentrations as a function of the oxidation state for pure ThO_2. Whereas in Figure 1 the vertical line "1" separates a net acidic from a net basic solvent, the intersection of lines in the center of the K–V diagrams separates the regions of dominance for either conduction electrons or positive holes at low P_{O_2} and high P_{O_2} respectively. It is informative to examine the equations that were applied simultaneously to derive Figure 4 for pure thoria, which exhibits interstitial anions and vacant anion sites:

$$\text{Native defect equilibrium: } O_O^x = O_i'' + V_O^{\cdot\cdot} \quad [4]$$

$$\log [O_i''] + \log [V_O^{\cdot\cdot}] = \log K_n \quad [4']$$

$$\text{Intrinsic electronic equilibrium: } 0 = e' + h^{\cdot} \quad [5]$$

$$\log [e'] + \log [h^{\cdot}] = \log K_i \quad [5']$$

$$\text{Environmental equilibrium: } 1/2O_2\,(g) = O_i'' + 2h^{\cdot} \quad [6]$$

$$\log [O_i''] + 2\log[h^{\cdot}] - 1/2 \log P_{O_2} = \log K_e \quad [6']$$

Electrical neutrality condition:

$$[h^{\cdot}] + 2[V_O^{\cdot\cdot}] = [e'] + 2[O_i''] \quad [7]$$

According to K–V defect notation, the principal character refers to the species or defect under consideration, the subscript to the relevant site, and the superscript to the charge of the species or defect relative to normal site occupation (dots for positive and primes for negative relative charges). Brackets refer to concentrations, *e.g.*, in number/cm^2 or in site fraction.

If the values of the three equilibrium constants are known, which is not usual, a computer can readily solve Eqs. [4′] through [7] to determine the four unknown concentrations for a given value of P_{O_2}. In the absence of known equilibrium constants, an informative examination of these equilibria is offered by Figure 4, which plots all the conceivable equilibrium conditions as a function of P_{O_2}.* To construct Figure 4, three different pairs of positive and negative defects from the electrical neutrality condition (ENC) are assumed to dominate over a given regime of oxygen activity, with $[O_i'']$ = $[V_O^{\cdot\cdot}]$ at exact stoichiometry because $K_n >> K_e$. There are several analogies between the Figure 3 plot of solute concentrations in an aqueous solution and Figure 4 for defect concentrations in pure ThO_2: the centerline of Figure 2 corresponds to a neutral solvent, while the center of Figure 4 indicates a stoichiometric compound. In each diagram, the slopes of the lines mapping solute concentrations are decided by the stoichiometric coefficients in the relevant equations describing equilibrium, while the placements of the lines are fixed by the magnitudes of the equilibrium constants.

*For convenience, the central zone of Figure 4 has been drawn quite narrow, but normally at the stoichiometric condition, the ionic defect concentrations would be several (or many) orders of magnitude higher than the electronic defect concentrations.

With Figure 4 as a description of pure ThO_2, the significant change in the defect concentrations caused by the dissolution of an electrically active (aliovalent) solute can be treated by a change in the ENC, *e.g.*, for Y_2O_3 dissolution as trivalent yttrium ions on tetravalent thorium sites (Y_{Th}'). For a sufficiently dilute and soluble Y_2O_3 addition, the equilibrium constants [1] through [3] remain the same, but the ENC becomes

$$\text{ENC: } [h^{\cdot}] + 2[V_O^{\cdot\cdot}] = [Y_{Th}'] + [e'] + 2[O_i''] \quad [7']$$

As for Figure 4, the new K–V diagram describing all conceivable dominant defect scenarios for ThO_2-Y_2O_3 solid solutions is plotted by again considering P_{O_2} zones, which are dominated by different pairs of the charged defects, as shown in Figure 5. In some respects, an aliovalent impurity for the solid compound resembles a complexing ion in a liquid ionic solution. But the effect of the complexing ion enters the mathematics by introducing a new equilibrium equation with another equilibrium constant, which provides another equation with the summation of log terms, while the aliovalent solute only enters the linear ENC.

As a second example for equilibria in defective crystalline compounds, for 15 to 20 years, the compound NiO was

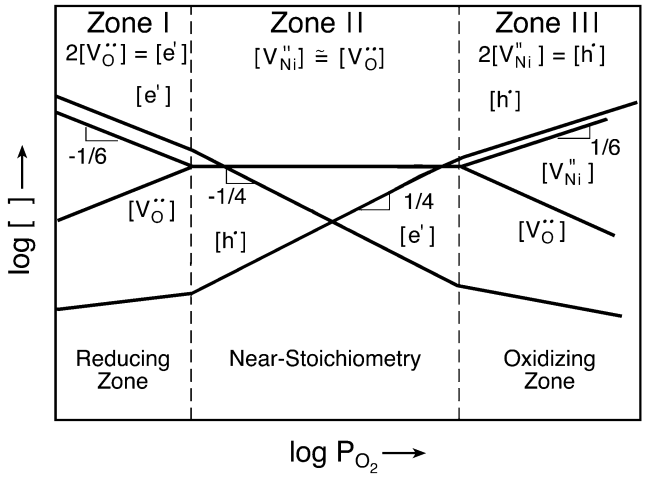

Fig. 6—K–V type diagram for defect concentrations in pure NiO.

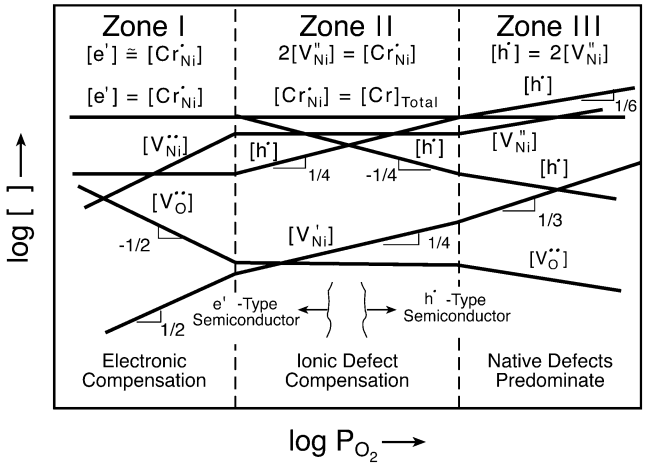

Fig. 7—K–V type diagram for defect concentrations in NiO-Cr_2O_3 solid solutions.[10]

considered in the ceramics and oxidation communities as a sort of prototype. The dominant point defects for this NaCl-type lattice are cation and anion vacancies described by the equilibria

$$\text{Native defect equilibrium: } 0 = V_{Ni}'' + V_O^{\cdot\cdot} \qquad [8]$$

$$\log [V_{Ni}''] + \log [V_O^{\cdot\cdot}] = \log K_n \qquad [8']$$

$$\text{Intrinsic electronic equilibrium: } 0 = e' + h^{\cdot} \qquad [9]$$

$$\log [e'] + \log [h^{\cdot}] = \log K_i \qquad [9']$$

Environmental equilibrium:

$$1/2\ O_2\ (g) = O_O^x + V_{Ni}'' + 2h^{\cdot} \qquad [10]$$

$$\log [V_{Ni}''] + 2 \log [h^{\cdot}] - 1/2 \log P_{O_2} = \log K_e \qquad [10']$$

$$\text{ENC: } [h^{\cdot}] + 2[V_O^{\cdot\cdot}] = [e'] + 2[V_{Ni}''] \qquad [11]$$

Upon following the same sort of simplification of the ENC by considering pairs of dominant positive and negative defects, the K–V diagram of Figure 6 can be drawn. Figure 6 permits the prediction of the dependencies on oxygen activity for the cation diffusivity and for the p-type electronic conductivity. As always, the K–V diagram covers all the conceivable defect scenarios, while only NiO with a net oxygen deficiency and *p*-type conduction really exists in the physical/experimental world.

The substitution of Cr_2O_3 into the NiO lattice has been of interest to understand why Ni-Cr alloys dilute in Cr oxidize faster than pure NiO, while Ni-20Cr alloy oxidizes at a much slower rate. To analyze the dissolution of Cr_2O_3 into NiO, the trivalent Cr dopant is introduced only into a new ENC Eq. [11], while the equilibrium constants of Eqs. [8′] through [10′] remain the same:

$$\text{ENC: } [h^{\cdot}] + 2[V_O^{\cdot\cdot}] + [Cr_{Ni}^{\cdot}] = [e'] + 2[V_{Ni}''] \qquad [11']$$

The resulting K–V plot of defect concentrations for NiO-Cr_2O_3 solid solutions is shown as Figure 7, which also takes into account a minority concentration of singly ionized cation vacancies. Clearly, the dissolution of trivalent Cr into NiO is compensated electrically by an increase in the cation vacancy concentration,[10] which explains why dilute Ni-Cr alloys oxidize faster. The fact that Cr^{3+} ions both create vacancies and use them for diffusion led to an interesting study of the concentration dependence of Cr diffusion in Cr-doped NiO.[11]

Incidentally, the treatment and presentation of the thermodynamic description for binary intermetallic compounds, as first treated by Wagner and Schottky,[4] does not follow the same format as that for semiconducting compounds. For binary intermetallic compounds, defect equilibria are described by expressions similar to Eq. [8], but substituted misplaced atoms also become possible point defects. An environmental equilibrium equivalent to Eq. [10] involves the activity of one of the metallic components. Expressions such as Eqs. [9] and [11] find no application, and an important effect from substituted impurities is not expected. Excellent experimental studies of the systems Fe-Al,[12] Ni-Al,[13] Cr-Al,[14] and Co-Al[15] were achieved by Komarek *et al.*

IV. EXTENSION OF METHOD TO OXYANION FUSED SALTS-SODIUM SULFATE

In 1968 to 1969, I was a member of an NMAB committee of High-Temperature Corrosion of Superalloys. The specific problem under analysis involved the accelerated oxidation of aircraft gas turbine components at high temperatures beneath a thin coating of fused Na_2SO_4. Sodium entered the combustion gas stream principally in a seawater aerospray and sulfur was an unavoidable impurity in the fuel. The fused salt sodium sulfate has a high thermodynamic stability, which is satisfied by even the low P_{SO_3} in the combustion product gases. A fused salt film could be deposited wherever the hardware had a temperature below the dew point for sodium sulfate, which was generally around 1050 °C. At that time, the mechanism was so poorly understood that the initial name for the phenomenon was “sulfidation.” However, as shown later by Goebel and Pettit,[16,17] Bornstein and DeCrescente,[18,19] and Luthra and Shores,[20] the accelerated attack resulted from a reaction of the metallic substrate with the fused salt film and not directly with sulfur-containing molecules in the gas phase. Thus, the reaction mechanism resembles aqueous atmospheric corrosion in many ways, and the problem is now called “hot corrosion”.[21–23]

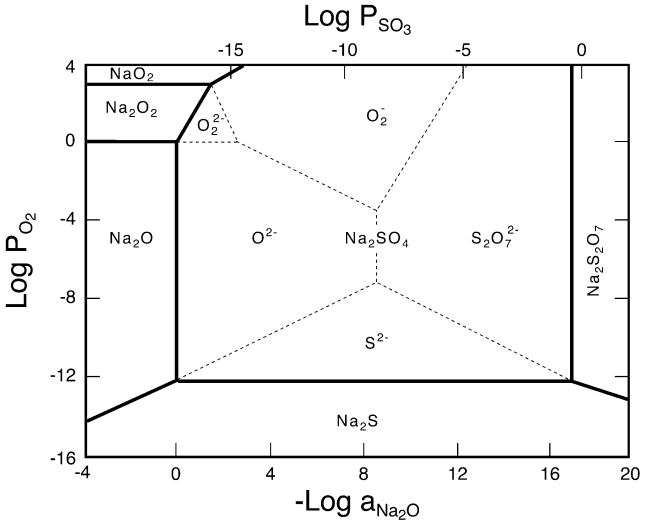

Fig. 8—Na-S-O phase stability diagram for 900 °C.[24]

Lacking any show of interest by fused salt chemists, we began to study hot corrosion by the design and use of electrochemical reference electrodes for measurements of the thermodynamic activities of sodium and oxygen to achieve a knowledge of melt basicity, and by the measurement of some oxide solubilities in fused sodium sulfate. I was not aware of it at the time, but we had simply started to extend the Pourbaix approach for aqueous equilibria to a high-temperature fused salt system. Later, this analogy became apparent and we plotted a phase stability diagram for the pure solvent, fused Na_2SO_4, following the Pourbaix format.[24] Figure 8 shows a broad central field of stability for Na_2SO_4 in the Na-S-O system at 1173 K, with minority solutes of O^{2-}, O^{2-},O_2^{2-}, $S_2O_7^{2-}$ and S^{2-} in the indicated fields. Analogous to the Pourbaix diagrams of Figures 1 and 2, the abscissa indicates a measure of melt basicity, defined as log a_{Na_2O} for fused Na_2SO_4. Unfortunately, the pioneers in describing the acid/base behavior of fused salts may not have realized their connection to the earlier work of Pourbaix, and they began plotting increasing acidity with increasing abscissa values, the opposite of the convention for aqueous solutions. Therefore, Figure 8 and all succeeding plots for fused salts are a sort of mirror image of the Pourbaix diagrams, but their significance and information are the same.

To investigate the solubilities in fused Na_2SO_4 for a given metal oxide system, *e.g.*, iron-oxide, the Fe-O-S (Ellingham) phase stability diagram can be superimposed over the field for sodium sulfate stability (Figure 8) to provide a stability diagram for the Na-Fe-S-O system (Figure 9). In effect, one is now examining the mutual compatibility for the compounds of iron in fused Na_2SO_4. In Figure 9, there is no set of conditions where metallic iron enjoys a stable existence with the fused salt, so clearly a corrosion reaction must be expected when iron contacts fused Na_2SO_4. In analog to Figure 2, Figure 9 shows that at high oxygen activities, Fe_2O_3 should dissolve as either a basic solute FeO_2^- in basic melts or as a trivalent acidic solute Fe^{3+} in acid melts. In very basic melts, the $NaFeO_2$ phase, and not Fe_2O_3, is stable. At lower oxygen activities, Fe_3O_4 would dissolve as either FeO_2^- or else as the divalent acidic solute Fe^{2+}. At extremely low oxygen activities, ferrous sulfide is stable.

At high oxygen activity, *e.g.*, 1 atm O_2:

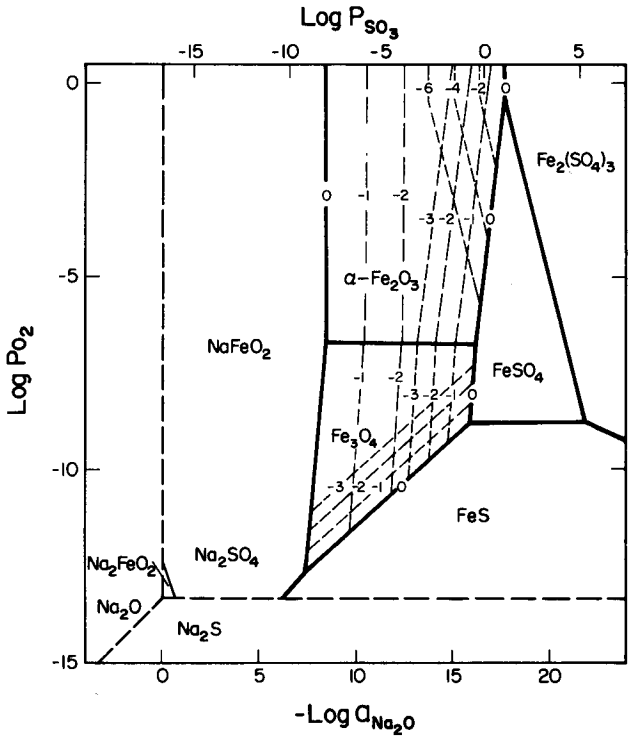

Fig. 9—Na-Fe-S-O phase stability diagram for 1200 K.[25]

Basic dissolution: $Fe_2O_3 + Na_2O = 2NaFeO_2$ [12]

$$d \log [NaFeO_2]/d(-\log a_{Na_2O}) = -1/2 \quad [12']$$

In a very basic melt: $NaFeO_2 = NaFeO_2$ [13]

$$d \log [NaFeO_2]/d(-\log a_{Na_2O}) = 0 \quad [13']$$

Acidic dissolution:

$$Fe_2O_3 + 3Na_2SO_4 = 2Fe(SO_4)_{1.5} + 3Na_2O \quad [14]$$

$$d \log [Fe(SO_4)_{1.5}]/d(-\log a_{Na_2O}) = +3/2 \quad [14']$$

At low oxygen activity, *e.g.*, for $P_{O_2} < Fe_2O_3$-Fe_3O_4 equilibrium:

Basic dissolution:

$$Fe_3O_4 + 3Na_2O = 3NaFeO_2 + 1/2O_2\,(g) \quad [15]$$

$$\partial \log [NaFeO_2]/\partial(-\log a_{Na_2O}) = -1 \text{ for fixed } P_{O_2} \quad [15']$$

$$\partial \log [NaFeO_2]/\partial \log P_{O_2} = -1/6 \text{ for fixed } a_{Na_2O} \quad [15'']$$

In a very basic melt: $NaFeO_2$ (solid)

$$= NaFeO_2 \text{ (solute)} \quad [16]$$

$$d \log [NaFeO_2]/d(-\log a_{Na_2O}) = 0 \quad [16']$$

Acidic dissolution:

$$Fe_3O_4 + 3Na_2SO_4 = 3FeSO_4 + 3Na_2O + 1/2O_2\,(g) \quad [17]$$

$$\partial \log [FeSO_4]/\partial(-\log a_{Na_2O}) = +1 \text{ for fixed } P_{O_2} \quad [17']$$

$$\partial \log [FeSO_4]/\partial \log P_{O_2} = -1/6 \text{ for fixed } a_{Na_2O} \quad [17'']$$

At very low oxygen activity, where FeS is the acidic solute:

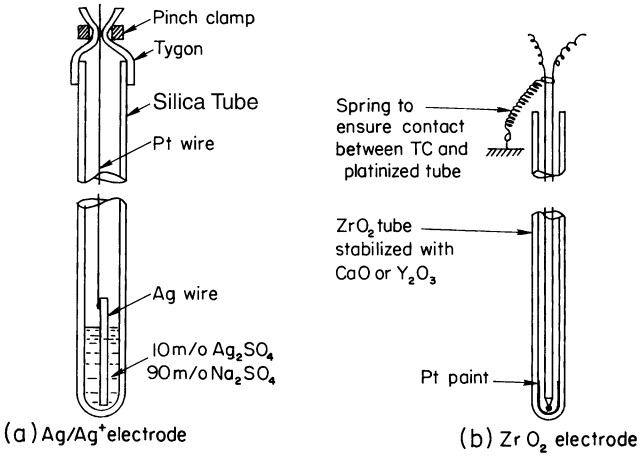

Fig. 10—(*a*) and (*b*) Experimental EC reference electrodes to measure simultaneously sodium and oxygen activities and thereby melt basicity.[24]

Acidic dissolution: $Fe_3O_4 + 3Na_2SO_4$

$$= 3FeS + 3Na_2O + 13/2O_2\ (g) \quad [18]$$

$$\partial \log [FeS]/\partial\ (-\log a_{Na_2O}) = 1 \text{ for fixed } P_{O_2} \quad [18']$$

$$\partial \log [FeS]/\partial \log P_{O_2} = -13/6 \text{ for fixed } a_{Na_2O} \quad [18'']$$

Before proceeding to experimental testing, let me generalize about this procedure for making "predictions" for the solubilities of compounds as a function of the melt basicity and oxygen activity. First, this approach has all its features common to the Pourbaix formalism for aqueous solutions and much in common with the K–V treatment of point defect equilibria in solid compounds. To plot Figures 8 and 9, one needs only to know the identity of the stable compounds in the system and their standard Gibbs energies of formation for the temperature of interest. Today, this information and the plotting capability are available on computer software. Each compound might be expected to exhibit at least one acidic solute and one basic solute, although obviously for the iron oxides of Figure 9, there are three different acidic solutes but only one basic solute. The predicted dependence of any solubility on basicity is decided by the stoichiometric coefficients in the balanced dissolution reaction. If a valence change is involved in any dissolution reaction, then the solubility will exhibit a predictable dependence on oxygen activity, otherwise not. Finally, for dilute solutions, the activities of solutes can be equated to their concentrations (Henrian solutions), or if ideal solutions are assumed for the solutes in the solvent, the calculations alone are sufficient to provide the magnitudes of the solubilities. Or, upon comparing the experimentally determined solubilities with those calculated, one establishes the Raoultian activity coefficients for the solutes.

To evaluate the predictions of Eqs. [12] through [18] experimentally, we developed and demonstrated the use of closed-end tubes of stabilized zirconia and impure silica as oxygen-ion and sodium-ion conducting solid electrolytes, as shown in Figure 10. These permitted the simultaneous measurement of oxygen and sodium activities in the fused Na_2SO_4 melt. Without repeating the previously published derivation,[22–24] the melt basicity (defined as log a_{Na_2O}) was given by the open-circuit voltage between the two sensing electrodes:

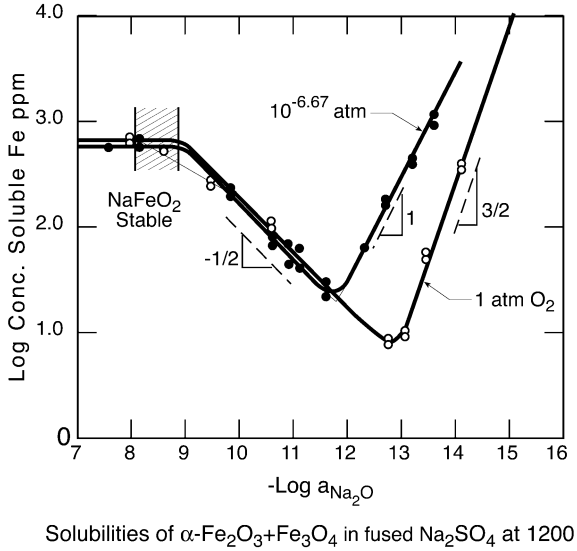

Fig. 11—Experimentally measured solubilities for iron oxides in fused pure Na_2SO_4 at 1200 K.[25]

Table I. Experimentally Determined Raoultian Activity Coefficients for Dilute Solutes in Fused Na_2SO_4[25,26]

Dissolved Oxide	Acidic Solutes	Basic Solutes
Fe_2O_3, Fe_3O_4	$Fe_2(SO_4)_3$ 0.0036	$NaFeO_2$ 430
	$FeSO_4$ 0.83	
	FeS 180	
Cr_2O_3	$Cr_2(SO_4)_3$ 5.8	Na_2CrO_4 4.6
	CrS 20.5	$NaCrO_2$ 2.3
Al_2O_3	$Al_2(SO_4)_3$ 2.3	$NaAlO_2$ 3.6
Co_3O_4, CoO	$CoSO_4$ 2.5	$NaCoO_2$ —
NiO	$NiSO_4$ 0.12	$NaNiO_2$ 50
CeO_2	$Ce(SO_4)_2$ —	Na_2CeO_3 —

At 1173 K: $E = -1.466 - 0.116 \log a_{Na_2O}$ [19]

By the withdrawal and analysis of samples from oxide-saturated melts, at known, measured values for log a_{Na_2O}, the solubilities of oxides in fused sodium sulfate could be determined by atomic absorption spectrophotometry. For example, the acidic and basic solubilities of iron oxides were measured for comparison with the forelying predictions. These results are presented in the log-log plot of Figure 11 for both 1 atm of oxygen and for a low oxygen activity corresponding to Fe_3O_4-Fe_2O_3 equilibrium.[25] In each case, the dependencies of the experimental solubilities on melt basicity (slopes of lines) are in excellent agreement with the predictions, indicating the utility of the methods. In very basic melt conditions, the solubility does not depend upon melt basicity because the compound $NaFeO_2$ becomes the stable phase, as described by Eqs. [16] and [16′]. The magnitudes for the Raoultian activity coefficients for the solutes in the Na-Fe-S-O system are presented in Table I. A change of 20,740 J for the combined standard Gibbs energies for Eq. [17], for example, would account for a factor two change in the activity coefficient for the acidic ferrous solute. So the calculated activity coefficients should not be considered very accurate. Figure 12 presents a "master plot" of solubilities for the iron oxides in fused Na_2SO_4, covering the entire

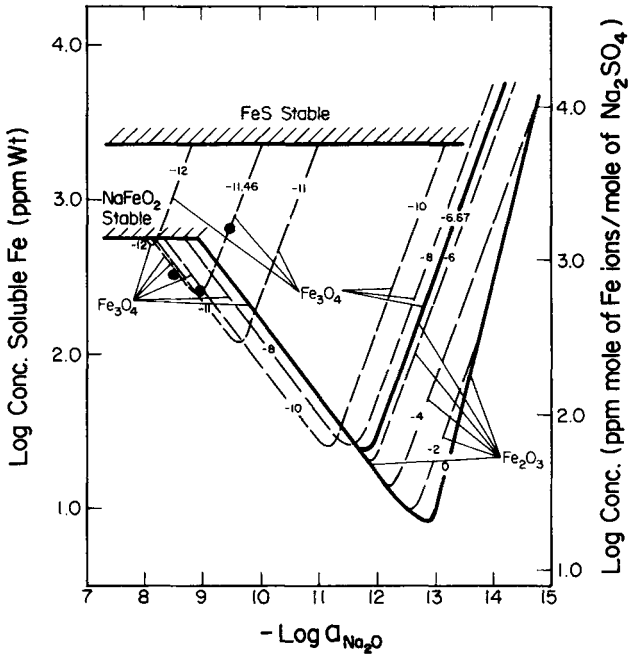

Fig. 12—Map of solubilities for iron oxides for all values of melt basicity and oxygen activity.[25]

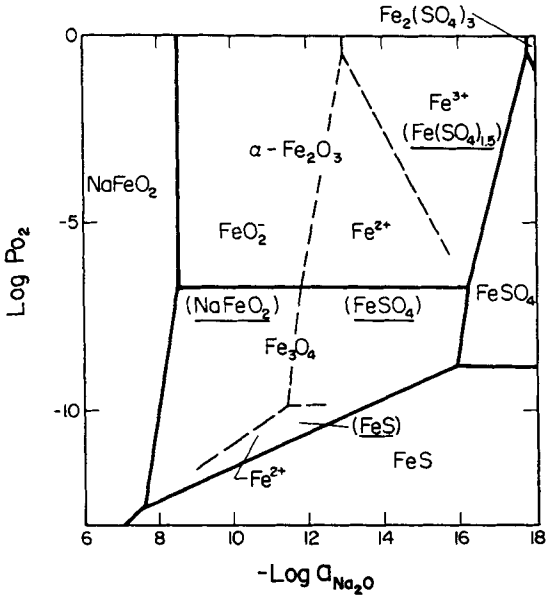

Fig. 13—Dominant iron solute species in the iron oxide-Na_2SO_4 system at 1200 K.[25]

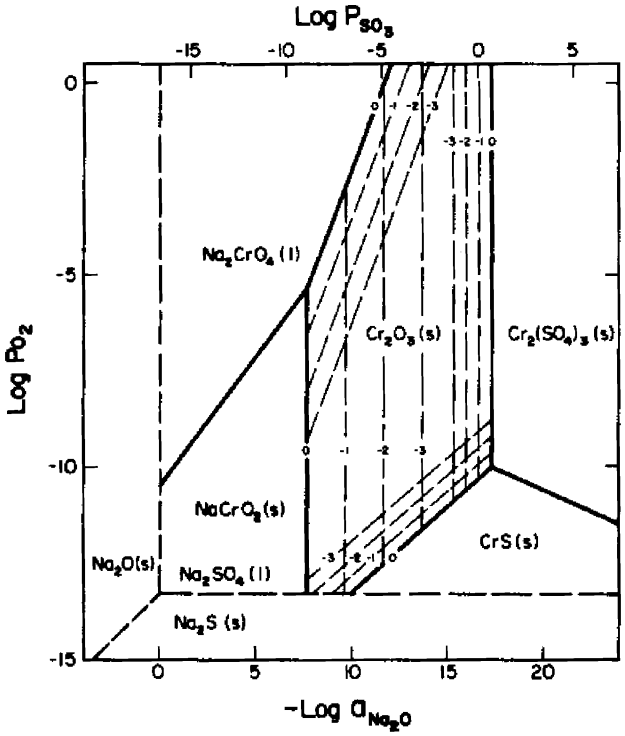

Fig. 14—Na-Cr-S-O phase stability diagram for 1200 K.[26]

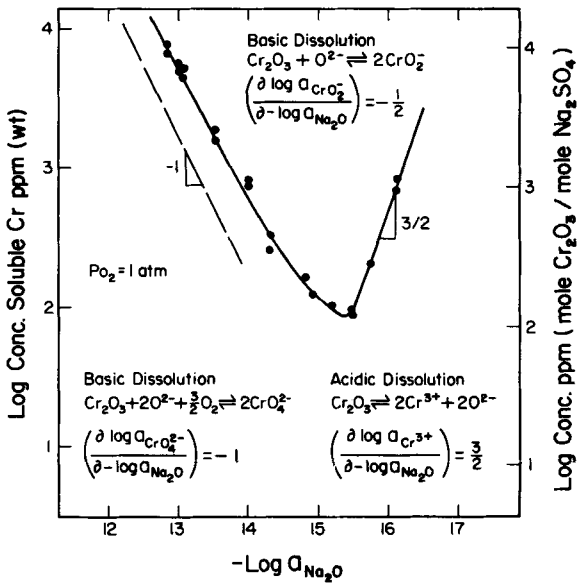

Fig. 15—Experimentally measured solubilities for chromium oxide in fused pure Na_2SO_4 at 1200 K and 1 atm oxygen.[26]

range of values for melt basicity and oxygen activity.[25] Three more experimental points for conditions where FeS is the acidic solute (Eqs. [18′] and [18″]) are added in confirmation of the analyses. Following the Pourbaix approach, Figure 13 presents a superposition onto Figure 9 of dotted lines mapping the fields of dominant solute species in the iron oxide-Na_2SO_4 system at 1200 K.

Chromium oxide is another interesting oxide, which is important to the protection of alloys from attack by fused sodium sulfate. Figure 14 presents the superposition of the Ellingham phase stability plot for Cr-S-O onto the Na-S-O phase stability diagram to analyze the compatibility of Cr_2O_3 in fused Na_2SO_4 at 1200 K. In this case, the single oxide Cr_2O_3 can dissolve as two acidic solutes ($Cr_2(SO_4)_3$ and CrS) and two basic solutes (Na_2CrO_4 and $NaCrO_2$), these involving three different valence states for chromium. Dashed lines indicate the loci for solute activities of 10^{-1}, 10^{-2}, and 10^{-3}. Zhang[26] measured the solubilities of Cr_2O_3 at 1 atm and $10^{-11.5}$ atm oxygen to establish the results presented in Figures 15 and 16, respectively. The relevant dissolution reactions and the predicted dependencies on melt

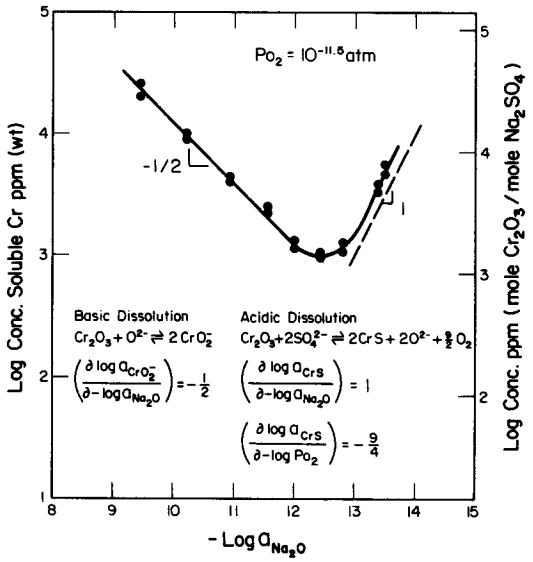

Fig. 16—Experimentally measured solubilities for chromium oxide in fused pure Na_2SO_4 at 1200 K and $10^{-11.5}$ atm.[26]

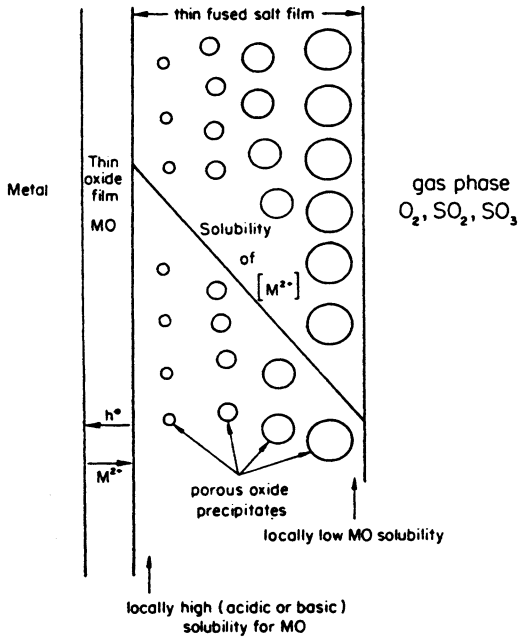

Fig. 17—Reprecipitation of porous MO oxide supported by a negative solubility gradient in the fused salt film.[28]

basicity and oxygen activity are indicated directly on Figures 15 and 16. The observed dependencies for the measured solubilities agree exactly with the predictions, although the specific solutes and slopes differ in the two plots. In Figure 15, in a range of intermediate basicity, the second basic solute $NaCrO_2$ is actually detected. In analog to Figures 12 and 13, Zhang[26] also published a master plot of solubilities and the dominant solute regimes for the dissolution of Cr_2O_3 in fused Na_2SO_4 at 1200 K. The calculated activity coefficients for the chromium solutes are compiled in Table I.

In the design of alloys to resist hot corrosion, chromium is known to be the most effective alloying element. In combination with studies of electrochemical kinetics,[27] the solubility behavior provides insight into the protective mechanism. In fact, the probable mechanism for hot corrosion in many instances is the existence of a "negative solubility gradient" for the oxide solute in the fused salt film.[28] Several experimental studies support this mechanism.[29–31] When the gradients in melt basicity and oxygen activity in the thin salt deposit are such that the solubility of the protective oxide is higher at the salt-oxide interface than at the salt-gas interface, then the protective oxide should dissolve at the oxide-salt interface and reprecipitate as a nonprotective porous particle in the salt film, as illustrated schematically in Figure 17. Because Cr_2O_3 is such an acidic oxide, the formation of basic chromate ions is generally its dissolution mechanism. But because of the positive power dependence for chromate solubility on oxygen activity, the solubility for chromate increases in the direction of the salt-gas interface, so that the negative solubilty gradient is not satisfied. Rather, any chromate ions existing closer to the salt-gas interface are expected to diffuse back toward the oxide-salt interface, where they may precipitate on the surface to provide some protection.[32] Incidentally, the same mechanism is believed to describe the effectiveness of oxidizing inhibitors (chromates, molybdates) for corrosion in aqueous solutions.

Solubility studies as outlined here for the iron oxides and for chromium oxide were also carried out in pure Na_2SO_4 at 1200 K for other important oxides, namely, NiO,[33] Co_3O_4,[33] Al_2O_3,[34] SiO_2,[35] and CeO_2,[36] as presented in

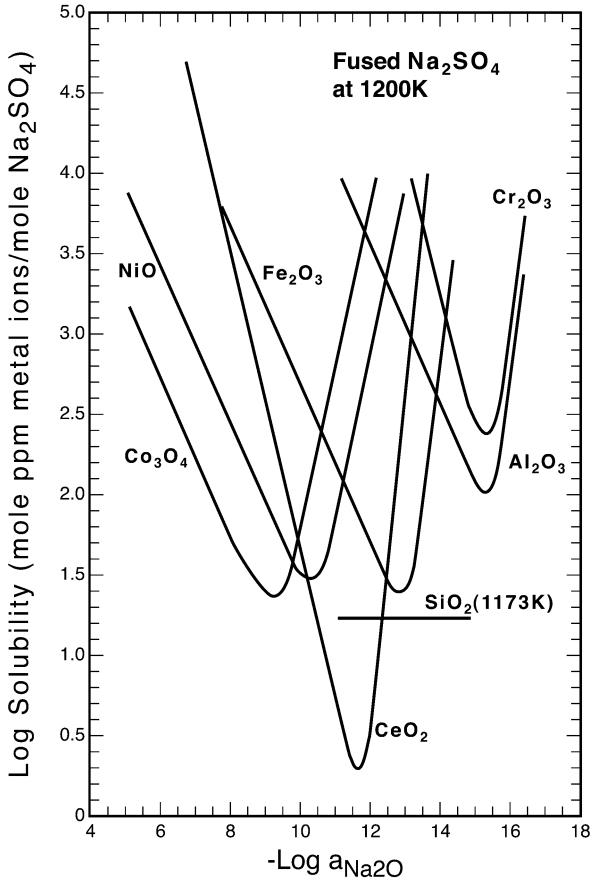

Fig. 18—Compilation of measured solubilities for several oxides in fused pure Na_2SO_4 at 1200 K.[22,23]

Figure 18. Raoultian activity coefficients for all these oxides are found in Table I. In addition, the theory is available for

the analysis of the solubility for a ternary compound.[33] Figure 18 provides a wealth of quantitative data relevant to the hot corrosion of high-temperature alloys. First, the minima in the solubilities between the most basic oxides Co_3O_4 and NiO compared to those for the most acidic oxides Cr_2O_3 and Al_2O_3 are separated by about six orders of magnitude. The operating conditions for a gas turbine correspond roughly to the basicity where Cr_2O_3 and Al_2O_3 enjoy their minimum solubilities, and alloys and coatings containing high Cr and Al are the most suitable for protection against hot corrosion. As an exception to the usual behavior, the solubility for SiO_2 exhibits no dependence upon melt basicity within the experimental range. This indicates a molecular solute for silica whose formation reaction does not involve oxide ions. If, in practice, the basicity of a salt film should reside between the minima of oxides for two alloying components, then a sort of "synergistic hot corrosion" should occur with mutual support for the acidic dissolution of the basic oxide(s) and basic dissolution for the acidic oxide. Experiments[37] on the kinetics of mutual dissolution of Fe_2O_3 and Cr_2O_3 have supported this model for synergistic hot corrosion. These comments about the application of solubility data to hot corrosion are made to illustrate their importance to interpret practical problems.

The hot corrosion field is also aware that vanadates are among the most corrosive components in fused salts, *e.g.*, as a solute in fused Na_2SO_4. While part of the problem lies with the role of vanadates in lowering the liquidus of the melt, another problem is introduced by the tendency of these strong acids to complex oxide ions, according to the following equilibria:[38]

$$Na_2SO_4 = Na_2O + SO_3 \qquad [20]$$

$$Na_3VO_4 = Na_2O + NaVO_3$$
$$K_{21} = a_{Na_2O}[NaVO_3]/[Na_3VO_4] \qquad [21]$$

$$2NaVO_3 = Na_2O + V_2O_5$$
$$K_{22} = aNa_2O\,[V_2O_5]/[NaVO_3]^2 \qquad [22]$$

The analysis to understand vanadate solutions again follows the Pourbaix format for aqueous solutions. First, because the standard Gibbs energies for Reactions [21] and [22] are known, a thermodynamic stability diagram for the Na-V-O system can be superimposed on the stability diagram for Na_2SO_4, as shown in Figure 19. If one considers a solution of 0.7 Na_2SO_4-0.3$NaVO_3$ at 900 °C, and assumes ideal solution behavior, the thermodynamic stabilities for the orthovanadate Na_3VO_4, metavanadate $NaVO_3$, and V_2O_5 can be plotted on a linear ordinate scale, as shown in Figure 20. The individual stabilities of the several compounds are sufficiently different to provide individual dominance regimes. If these same data are plotted using a logarithmic ordinate scale, as seen in Figure 21, these equilibria for the fused salt solution have the appearance of a K-V plot for point defect concentrations in crystalline compounds (Figures 4 and 6). Indeed, for both solutions, a set of simultaneous equilibrium equations are solved, but instead of a linear ENC such as Eqs. [7], [7′], [11], or [11′], the fused salt solution has a linear expression for the vanadium mass balance:

$$n_V = n_{Na_3VO_4} + n_{NaVO_3} + 2n_{V_2O_5} \qquad [23]$$

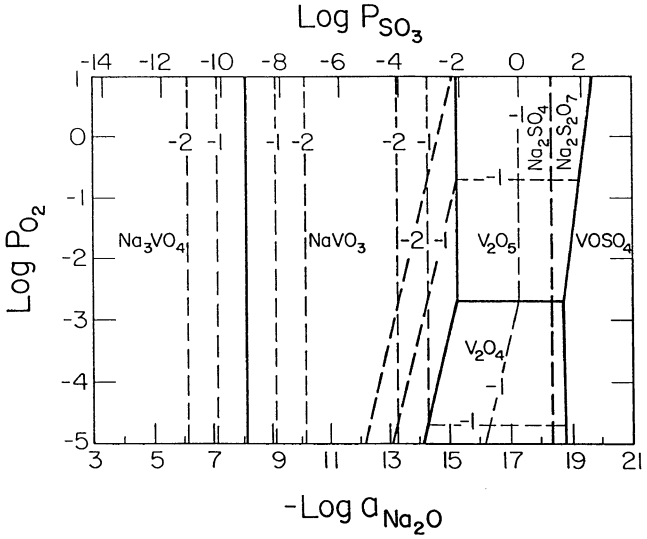

Fig. 19—Phase stability diagram for Na-V-S-O system at 900 °C.[38]

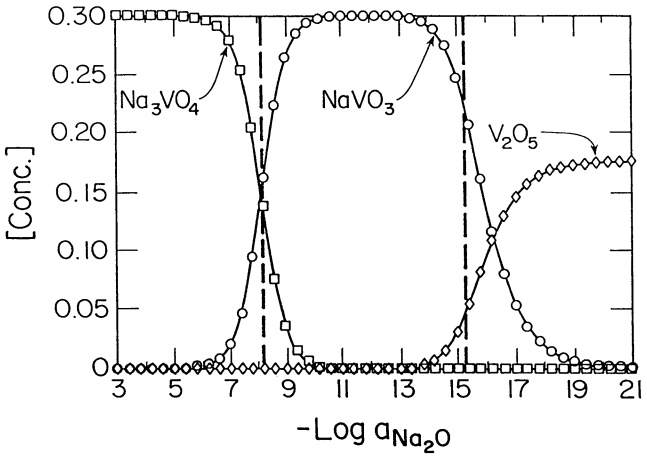

Fig. 20—Linear plot of equilibrium concentrations of vanadates in ideal solution of fused 0.7Na_2SO_4-0.3$NaVO_3$ at 900 °C.[38]

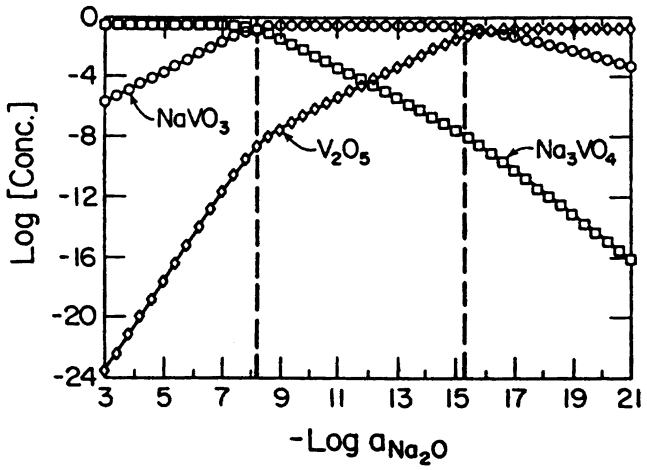

Fig. 21—Logarithmic plot of equilibrium concentrations of vanadates in ideal solution of fused 0.7Na_2SO_4-0.3$NaVO_3$ at 900 °C.[38]

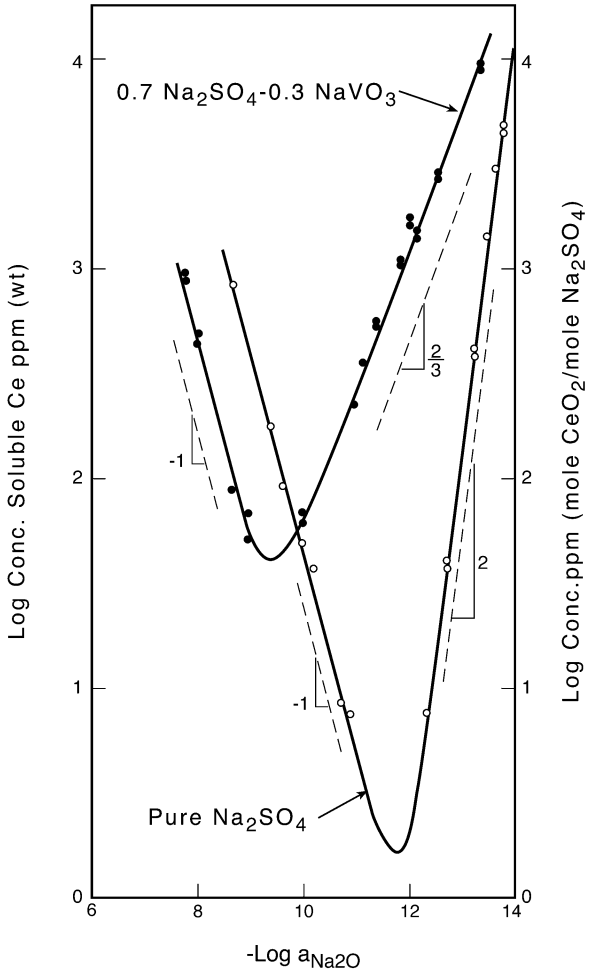

Fig. 22—Measured solubilities for pure CeO_2 in pure fused Na_2SO_4 and in fused $0.7Na_2SO_4$-$0.3NaVO_3$ at 900 °C.[36]

So the graphical description of equilibria for fused salts resembles that for crystalline compounds because the analyses are similar mathematically. Specifically, in each case, a set of equations involving the summation of logarithmic terms, which arise from equilibrium constants, is solved simultaneously with one equation containing only linear terms.

In an attempt to clarify the deleterious effect of vanadates in hot corrosion, the solubilities of the oxides HfO_2, CeO_2, and Y_2O_3 at 1200 K were determined as a function of basicity for a melt of $0.3NaVO_3$-$0.7Na_2SO_4$.[36] The activities of sodium and oxygen were again determined using the same electrochemical probes. The measured solubilities for these oxides in the sulfate-vanadate solutions were very well behaved, each with one acidic solute and one basic solute, but the magnitudes for the acidic solubilities seemed quite high, and their minima on a solubility plot were situated at quite high values of melt basicity. Thus, the solubility of CeO_2 in pure fused Na_2SO_4 was measured for comparison, resulting in Figure 22. The measurements of Figure 22 show that the presence of the strong acidic metavanadate causes a huge increase in the acidic solubility of ceria, up to nearly three orders of magnitude. The expression that describes the complexing of the oxide ion by the metavanadate would be valid for any oxide, not just ceria:

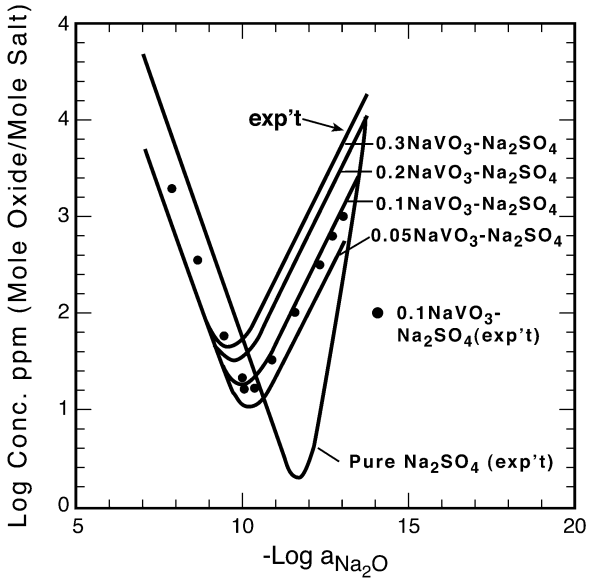

Fig. 23—Solubilities of CeO_2 in pure Na_2SO_4 and in Na_2SO_4-$x$$NaVO_3$ solutions at 900 °C in 1 atm O_2 (x = 0.3, 0.2, 0.1, and 0.05).[39]

$$3CeO_2 + 4NaVO_3 = Na_2O + Ce_3(VO_4)_4 \qquad [24]$$

Thus, the vanadates are expected to increase greatly the acidic solubility of every oxide, certainly an important factor in promoting hot corrosion atttack. Because the measurements of the acidic solubility for CeO_2 in the $0.3NaVO_3$ solution proved to be consistent with ideal solution behavior for the sulfate-vanadate melt, calculations could be made to predict the solubility of ceria for other solvent melt concentrations: 5, 10, and 20 mole pct $NaVO_3$ solutions, as shown in Figure 23. To prove the validity of this approach, the experimental measurements of ceria solubility in fused $0.9Na_2SO_4$-$0.1NaVO_3$ solution at 900 °C shown in Figure 23 are in excellent agreement with the calculations.[40] The method was extended to treat the solubilities of many other oxides in vanadate solutions.[38]

V. REVISION OF THE METHOD TO ANALYZE OTHER IONIC SOLUTIONS

The studies described in Section IV involved various melts comprising only one cation, sodium, but one or more anions, including sulfate, vanadate, chromate, and molybdate. In every case, the reference electrodes illustrated in Figure 10 functioned without problems to provide exact measurements of the thermodynamic activity for Na_2O, making log a_{Na_2O} a useful and unambiguous measure of the melt basicity. One can pose the question: "How would you measure and interpret the acid-base character of a melt comprised of only one anion, but a mixture of cations?" The practical necessity to answer this question arose as we considered the problem of the hot corrosion attack of steel heat exchange tubes (in a coal-fired boiler) by fly-ash condensate, which has a nominal composition of 71.2 mole pct Na_2SO_4, 17.8 mole pct K_2SO_4, and 11 mol pct Fe_2SO_4.[40] A reference electrode of the "hole-in-tube" geometry was adapted, as illustrated in Figure 24. Within the reference electrode (RE), the mixed cation sulfate is equilibrated with pure Fe_2O_3, which for a given melt composition fixes a specific value for P_{SO_3} from the equilibrium:

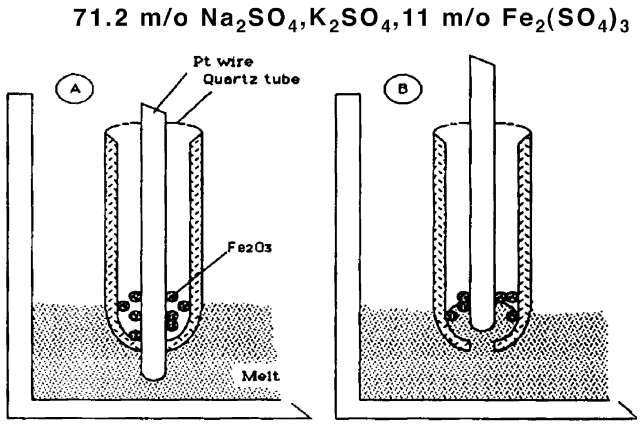

$$SO_3 + 1/2\ O_2 + 2e^- = SO_4^{2-}$$

$$Emf = -\frac{RT}{2F} \ln \frac{(P_{SO_3})_{RE}}{(P_{SO_3})_{WE}} - \frac{RT}{4F} \ln \frac{(P_{O_2})_{RE}}{(P_{O_2})_{WE}}$$

Fig. 24—(*a*) and (*b*) Reference electrode to measure the acid-base character for fused sulfate salt with mixed cations.[40]

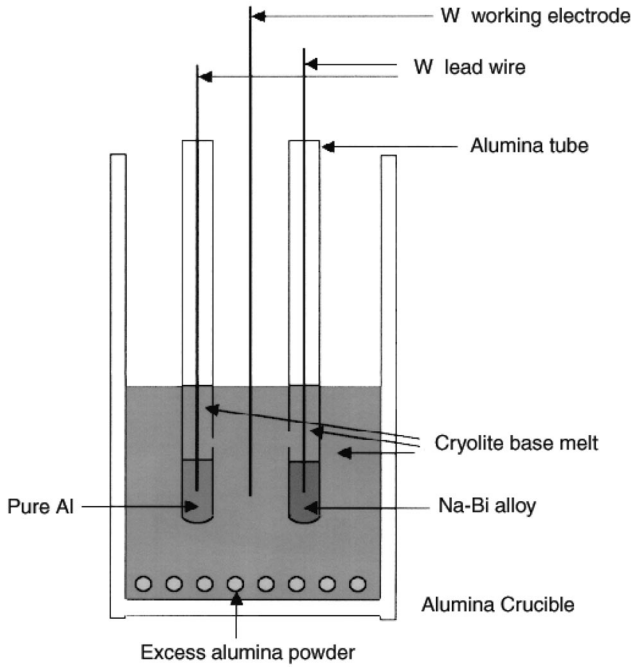

Fig. 25—Reference electrodes to measure the acid-base character for cryolite-based melts, fused fluoride with mixed cations.

$$Fe_2O_3 + SO_3\ (g) = Fe_2(SO_4)_3 \qquad [25]$$

But at a Pt working electrode (WE) contacting the bulk melt, the salt is not saturated with Fe_2O_3 and therefore exhibits a different P_{SO_3}, which is indicative of the melt acidity:

$$\text{At the WE: } SO_3\ (g) + 1/2\ O_2\ (g) + 2e- = SO_4^{2-} \qquad [26]$$

Then, for such a solution, the melt acidity can be defined as log P_{SO_3}, which would be obtained from a measurement of the electromotive force (emf) between the RE and the WE:

$$E = -RT/2F \ln (P_{SO_3})_{RE}/(P_{SO_3})_{WE} \quad \text{for same } P_{O_2} \text{ at RE and WE} \qquad [27]$$

At 963 K, such an acidity sensor for fused fly ash exhibited a linear calibration with various known P_{SO_3} gases, and it responded rapidly to changes in the gas composition.[40] This acidity sensor was also used to establish the solubilities of Cr_2O_3 and SiO_2 in the fused fly-ash condensate, and the predicted slopes for the expected solutes were obtained.[40] In the aggressive fly-ash condensate, the measured solubilities for Cr_2O_3 and SiO_2 at 963 K exceeded those in pure Na_2SO_4 at 1200 K by factors of about 6 and 3, respectively.

VI. EXTENSION OF THE METHOD TO CRYOLITE-BASE SOLUTIONS

The patenting of the Hall–Heroult cell (HHC) in 1886 for electrowinning primary liquid aluminum at about 960 °C and the use of this process up to the present has provided great technological progress to the world. The basis for the operation of the HHC was the discovery that the fused salt cryolite, Na_3AlF_6, is an effective solvent for alumina, Al_2O_3. But after more than a century of research, the acid-base behavior of cryolite has not been quantified and detailed mechanisms for the dissolution of alumina and other oxides in cryolite are lacking.[41] In other words, there in no plot equivalent to Figure 18 for oxide solubilities in cryolite-base melts, which are generally presented as a table lacking any connection to an acid-base character of the melt. This status is particularly troublesome as the industry continues efforts to develop a nonconsumable oxide or cermet anode where molecular oxygen can be evolved without excessive dissolution.

In an attempt to clarify this picture of oxide solubilities in cryolite, perhaps the methods and interpretations summarized for fused alkali sulfate can be extended to cryolite, a ternary salt with one anion and multiple cations. First, one needs a working definition of melt acidity or basicity and the means to measure this experimentally. In analog to the fly-ash condensate measurements,[40] the parameter log a_{AlF_3} should serve as a proper definition of melt acidity. Then to measure and know the acidity for such a melt, a pair of electrochemical reference electrodes are required (for a pure cryolite melt or one with known cryolite activity) to measure simultaneously two of the three elemental activities for Na, Al, or F. "Hole in tube" reference electrodes, as shown in Figure 25, are again suited to such measurements, and Haarberg and Egan[41] have demonstrated reference electrodes for the measurement of Al and Na activities in cryolite melts. In fact, the properties of cryolite as a strong acid effective at complexing oxide ions provides a similarity to the vanadates just discussed, except that the cryolite melts do not form such simple solutes, and with the introduction of dissolved oxides, the system becomes quaternary, not ternary. From Raman data[42] and other observations,[43,44] the dominant solute species are thought to be $Al_2OF_6^{2-}$ and $Al_2O_2F_4^{2-}$, but other complexes have also been suggested.

Zhang and I are starting research to measure and interpret the solubility of alumina and other oxides in a low-temperature basic cryolite melt containing 52 wt pct Na_3AlF_6, 38 pct NaF, 5 pct LiF and 5 pct CaF_2 at 900 °C. To proceed along the format previously discussed, Figure 26 provides

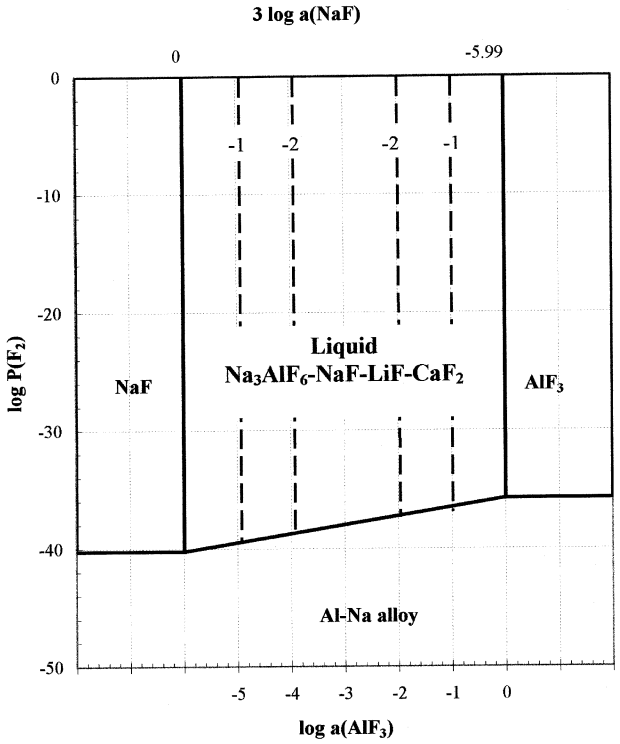

Fig. 26—Pourbaix-type diagram for NaF-rich NaF-Na_3AlF_6-LiF-CaF_2 system at 900 °C. (Activity of $Na_{0.5}Al_{0.167}F$ set equal to 0.548.)

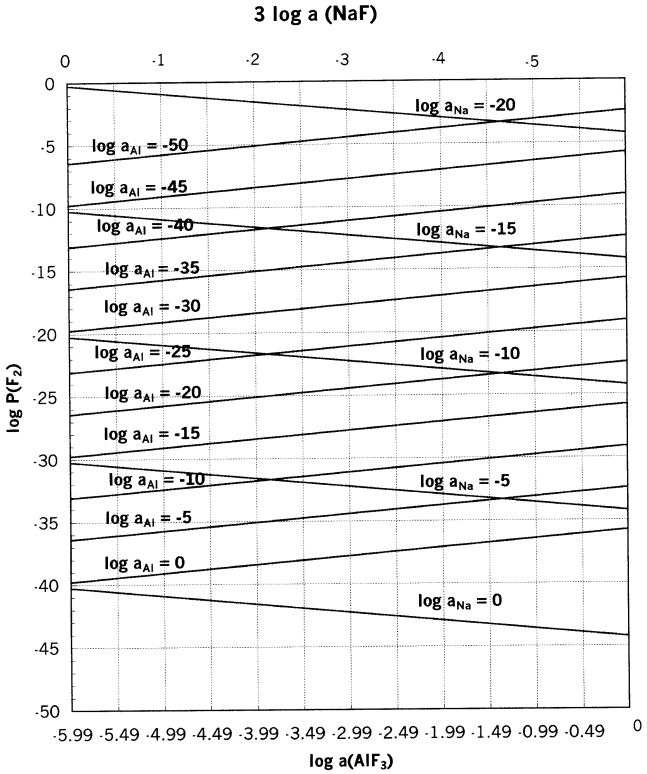

Fig. 27—Isoactivity lines For sodium and aluminum in stable cryolite field at 900 °C.

a Pourbaix-type plot for this cryolite-base melt at 900 °C where log a_{AlF_3} provides the quantitative measure for melt acidity. Figure 27 shows values for the thermodynamic activities for Na and Al within the liquid field, as can be measured by the reference electrodes of Figure 25. Obviously, a combined knowledge of these activities provides a known acidity (fixed point) on the diagram. Experimentally, melts will be brought to saturation with respect to excess alumina, or some other oxide, and samples will be withdrawn and analyzed to establish the relevant solubility. Additions or titrations to the melt should provide some shift in the melt acidity, so that the solubilities can be measured as a function of melt acidity, as has been done for aqueous solutions and for fused sodium sulfate.

The interpretation of the future solubility data should provide insight into the complex oxygen-containing solutes, since the dependencies of the solubility on melt acidity would be decided by the operative dissolution mechanism, *e.g.*, for alumina dissolution to form the two mentioned solutes:

$$2Na_3AlF_6 + Al_2O_3 + 2AlF_3 = 3Na_2Al_2OF_6 \text{ (acid solute)} \quad [28]$$

$$d \log [O]/d \log a_{AlF_3} = +2/3 \quad [28']$$

$$2Na_3AlF_6 + 2Al_2O_3 = 3Na_2Al_2O_2F_4 \text{ (neutral solute)} \quad [29]$$

$$d \log [O]/d \log a_{AlF_3} = 0 \quad [29']$$

for fixed cryolite activity and unit activity of alumina. If these two solutes enjoy comparable concentrations, then the resulting plot of solubility *vs* acidity will require some deconvolution. If the chosen reactions are not the correct ones, then no good fit to the data will result and other reactions must be proposed and tested. In any case, such data have not been previously collected for cryolite-base melts, and these experiments, in combination with other measurements and theory, could help to clarify the chemistry of cryolite solutions. In the absence of alumina, the acidic solubility of another oxide MO could be measured and interpreted:

$$2Na_3AlF_6 + 3MO + 4AlF_3 = 3Na_2Al_2OF_6 + 3MF_2 \quad [30]$$

$$d \log [M]/d \log a_{AlF_3} = +2/3$$

$$\text{because } [Na_2Al_2OF_6] = [M] \quad [30']$$

$$2Na_3AlF_6 + 6MO + 4AlF_3 = 3Na_2Al_2O_2F_4 + 6MF \quad [31]$$

$$d \log [M]/d \log a_{AlF_3} = +4/9$$

$$\text{because } 2[Na_2Al_2O_2F_4] = [M] \quad [31']$$

Analogous expressions can be written for oxides of other stoichiometries, *e.g.*, M_2O_3, M_3O_4, and MO_2. At the moment, a knowledge of the basic solutes for such oxides is lacking, but they might be identified (if applicable) from measured solubility curves. For the circumstance of practical interest, *i.e.*, the joint dissolution of alumina with another oxide, the analysis will became more complicated, because the simplifications of Eqs. [28′] through [31′] will not be valid. However, equations for mass balances for aluminum and for oxygen will help resolve the simultaneous solution for the relevant equilibrium constants. As was mentioned, these experimental studies are presently in progress.

VII. CONCLUSIONS

A comparison of the treatment of equilibria in several apparently quite different sorts of ionic solutions has shown that significant similarities in the analyses exist.

1. The mathematical analyses are similar, resulting in similar graphical representations.
2. The definition and measurement of parameters to quantify the acid-base behavior of the solutions, in addition to a defined and measurable oxidation state, provide the primary means to characterize the equilibrium state and predict concentration dependencies.
3. For liquid ionic solutions, electrochemical probes are effective in the measurement of the desired "state" parameters.
4. Balanced chemical equations involving the solvent, the solute, and the state parameters provide predictions concerning the solubilities of other phases, *e.g.*, solid oxides, in the solvent. The stoichiometric coefficients decide the solubility dependencies and the equilibrium constant fixes the solubility magnitude, assuming an ideal solution.
5. A comparison of the experimentally measured solubilities to those calculated assuming an ideal solution leads to values for the Raoultian activity coefficients for the solutes in the solvent.

ACKNOWLEDGMENTS

My selection to present this Lecture would not have been realized except for the patient instruction and encouragement by many outstanding teachers: R.E. Grace, R. Schuhmann, G.M. Pound, R.F. Mehl, C. Wagner, and M. Pourbaix. Likewise, I have learned from my colleagues at Ohio State University: M.G. Fontana, J.P. Hirth, G.R. St. Pierre, and R. Staehle, and also from B. Pieraggi and W.C. Setzer. Many industrious graduate students and postdoctoral researchers contributed careful measurements and clever interpretations to the subjects presented here: G.H. Meier, M.K. Lasker, C.O. Park, D.Z. Shi, N. Otsuka, D.K. Gupta, Y.S. Hwang, P.P. Leblanc, and especially Y.S. Zhang, who is also currently active in the aluminum chemistry study. Various portions of the research at OSU mentioned in this article were supported by DOE-BES, NSF, EPRI, GE, and currently by the DOE-OIT Aluminum Program under Agreement No. DE-FC07-99ID13813.

REFERENCES

1. M. Pourbaix: *Atlas of Electrochemical Equilibria in Aqueous Solutions*, NACE, Houston, TX, 1974.
2. *Equilibrium Diagrams; Localized Corrosion*, Electrochemical Society Proc., R.P. Frankenthal and J. Kruger, eds., Pennington, NJ, 1984, vol. 84-9.
3. J. Frenkel: *Z. Phys.*, 1926, vol. 35, pp. 652-59.
4. C. Wagner and W. Schottky: *Z. Phys. Chem.*, 1930, vol. B11, pp. 163-210.
5. C. Wagner: *Ann. Rev. Mater. Sci.*, R.A. Huggins, ed., Palo Alto, CA, 1977, vol. 7, pp. 1-22.
6. F.A. Kroger and H.J. Vink: in *Solid State Physics*, F. Seitz and D. Turnbull, eds., Academic Press, New York, NY, 1956, vol. 3, pp. 307-435.
7. F. Kroger: *The Chemistry of Imperfect Crystals*, North-Holland Publishing Co., Amsterdam, 1964.
8. M.K. Lasker and R.A. Rapp: *Z. Phys. Chem. NF*, 1966, vol. 35, pp. 198-221.
9. R.A. Rapp: *Thermodynamics of Nuclear Materials*, Vienna International Atomic Energy Agency, Vienna, 1967, pp. 559-85.
10. G.H. Meier and R.A. Rapp: *Z. Phys. Chem. NF*, 1971, vol. 74, pp. 168-89.
11. R. Perkins and R.A. Rapp: *Metall. Trans.*, 1973, vol. 4, pp. 193-205.
12. J. Eldridge and K.L. Komarek: *TMS-AIME*, 1964, vol. 230, pp. 226-33.
13. A. Steiner and K.L. Komarek: *TMS-AIME*, 1964, vol. 230, pp. 786-90.
14. W. Johnson, K. Komarek, and E. Miller: *TMS-AIME*, 1968, vol. 242, pp. 1685-88.
15. M. Ettenberg, K.L. Komarek, and E. Miller: *TMS-AIME*, 1968, vol. 242, pp. 1801-07.
16. J.A. Goebel and F.S. Pettit: *Metall. Trans.*, 1970, vol. 1, pp. 1943-54.
17. J.A. Goebel, F.S. Pettit, and G.W. Goward: *Metall. Trans.*, 1973, vol. 4, pp. 261-78.
18. N.S. Bornstein and M.A. DeCrescente: *TMS-AIME*, 1969, vol. 245, pp. 1947-52.
19. N.S. Bornstein and M.A. DeCrescente: *Metall. Trans.*, 1971, vol. 2, pp. 2875-83.
20. K.L. Luthra and D.A. Shores: *J. Electrochem. Soc.*, 1980, vol. 127, pp. 2202-10.
21. J. Stringer: *Ann. Rev. Mater. Sci.*, R.A. Huggins, ed., Palo Alto, CA, 1977, vol. 7, pp. 477-509.
22. R.A. Rapp: *Corrosion*, 1986, vol. 42, pp. 568-77.
23. R.A. Rapp and Y.S. Zhang: *J. Met.*, 1994, vol. 46, pp. 47-55.
24. C.O. Park and R.A. Rapp: *J. Electrochem. Soc.*, 1986, vol. 133, pp. 1636-41.
25. Y.S. Zhang and R.A. Rapp: *J. Electrochem. Soc.*, 1985, vol. 132, pp. 734-35; 1986, vol. 133, pp. 2498-2501.
26. Y.S. Zhang: *J. Electrochem. Soc.*, 1986, vol. 133, pp. 655-57.
27. D.Z. Shi and R.A. Rapp: *Werkstoffe Korr.*, 1990, vol. 41, pp. 215-26.
28. R.A. Rapp and K.S. Goto: in *Molten Salts*, R. Selman and J. Braunstein, eds., The Electrochemical Society, Pennington, NJ, 1979, pp. 159-77.
29. N. Otsuka and R.A. Rapp: *J. Electrochem. Soc.*, 1990, vol. 137, pp. 46-52.
30. H. Numata, A. Nishikata, and S. Haruyama: *Corrosion*, 1988, vol. 44, pp. 724-31.
31. K.L. Luthra: *Metall. Trans. A*, 1982, vol. 13, pp. 1853-64.
32. N. Otsuka and R.A. Rapp: *J. Electrochem. Soc.*, 1990, vol. 137, pp. 53-60.
33. D.K. Gupta and R.A. Rapp: *J. Electrochem. Soc.*, 1980, vol. 127, pp. 2194-2202; 1980, vol. 127, p. 2656.
34. P.D. Jose, D.K. Gupta, and R.A. Rapp: *J. Electrochem. Soc.*, 1985, vol. 132, pp. 735-37.
35. D.Z. Shi and R.A. Rapp: *J. Electrochem. Soc.*, 1986, vol. 133, pp. 849-50.
36. Y.S. Zhang and R.A. Rapp: *Corrosion*, 1987, vol. 43, pp. 348-52.
37. Y.S. Hwang and R.A. Rapp: *J. Electrochem. Soc.*, 1989, vol. 137, pp. 1276-80.
38. Y.S. Hwang and R.A. Rapp: *Corrosion*, 1989, vol. 45, pp. 933-37.
39. Y.S. Zhang and R.A. Rapp: *Proc. 9th Int. Symp. on Molten Salts*, The Electrochemical Society, Pennington, NJ, 1994, pp.
40. P.P. Leblanc and R.A. Rapp: *J. Electrochem. Soc.*, 1992, vol. 139, pp. L31-L32; 1993, vol. 140, pp. L41-L43.
41. G.M. Haarberg and J.J. Egan: *Ber. Bunsenges, Phys. Chem.*, 1998, vol. 102, pp. 000-000.
42. B. Gilbert, E. Robert, E. Tixhon, J.E. Olson, and T. Ostvold: *Light Metals*, J. Evans, ed., TMS, Warrendale, PA, 1995, pp. 181-94.
43. E.W. Dewing and J. Thonstad: *Metall. Mater. Trans. B*, 1997, vol. 28B, pp. 1089-93.
44. J. Bouteillon, J.C. Poignet, and J.J. Rameau: *J. Met.*, 1993, vol. 45, pp. 27-30.